nature water

Article

https://doi.org/10.1038/s44221-024-00232-7

Near-complete destruction of PFAS in aqueous film-forming foam by integrated photo-electrochemical processes

Received: 8 August 2023

Accepted: 12 March 2024

Published online: 01 May 2024

Check for updates

Yunqiao Guan[1], Zekun Liu[2], Nanyang Yang[1], Shasha Yang[1,3], Luz Estefanny Quispe-Cardenas[1,3], Jinyong Liu[2] ✉ & Yang Yang[1] ✉

Per- and polyfluoroalkyl substances (PFAS) are highly recalcitrant pollutants in the water environment worldwide. Aqueous film-forming foam (AFFF) used for firefighting is a major source of PFAS pollution. However, complete defluorination (that is, cleaving all C–F bonds into F^- ions) of PFAS by non-thermal technology is rare. The destruction of the PFAS mixture in the complex organic matrix of AFFF is even more challenging. Here we designed and demonstrated an ultraviolet/sulfite–electrochemical oxidation (UV/S–EO) process. The tandem UV/S–EO leverages the complementary advantages of UV/S and EO modules in the PFAS transformation mechanism and the engineering process design (for example, foaming control, chemical dosage and energy consumption). At ambient temperature and pressure, the UV/S–EO realized near-complete defluorination and mineralization of most PFAS and organics in AFFF (50–5,000 times diluted, containing up to 200 mg l^{-1} organic fluorine and 3,764 mg l^{-1} organic carbon). This work highlights the integration of molecular-level insight and engineering design towards solving the major challenges of AFFF water pollution.

Aqueous film-forming foam (AFFF) for the suppression of fuel fires is a major cause of widespread and heavy water environment pollution by per- and polyfluoroalkyl substances (PFAS)[1–6]. While substantial efforts have been taken for groundwater remediation, a proactive solution is to contain further PFAS pollution via safe disposal of AFFF stockpiles and decontamination of wastewater from firefighting system cleaning[7,8]. The ideal treatment goal is complete defluorination of all PFAS in AFFF. However, only hydrothermal approaches have achieved near-complete defluorination of AFFF under supercritical (for example, 590 °C, 237 atm, 0.1 M KOH, 1 min for 1:100 diluted AFFF)[9] and subcritical (for example, 350 °C, 163 atm, 5 M NaOH, 30 min for 1:2 diluted AFFF) conditions[10,11]. Therefore, a non-thermal and cost-effective technology for complete PFAS defluorination is still highly desirable.

Although information on AFFF ingredients remains largely proprietary, PFAS-based surfactants are generally composed of a fluoroalkyl moiety (R_F) and an organic moiety (R_O)[12–14]. The two moieties are connected by either sulfonamide (R_F–SO_2NH–R_O) or hydrocarbon (R_F–$(CH_2)_m$–R_O) telomer linkers. From the perspective of chemical degradation, most such surfactants can be hydrolysed or partially oxidized into perfluoroalkane sulfonates (PFSAs, C_nF_{2n+1}–SO_3^-), perfluorocarboxylates (PFCAs, C_nF_{2n+1}–COO^-) and fluorotelomers (FTs, C_nF_{2n+1}–$(CH_2)_m$–X). However, most non-thermal technologies reported so far cannot achieve complete defluorination of all PFAS structures. The degradability of individual PFAS depends on the specific molecular structure, particularly the end functional group and fluoroalkyl chain length[15,16]. For example, the homogeneous ultraviolet/sulfite (UV/S) treatment shows low efficiency in destroying short-chain FTs and PFSAs due to their low intrinsic reactivity with hydrated electrons (e_{aq}^-)[17,18]. Unless a cationic surfactant is added, the heterogeneous plasma treatment is not good at destroying short-chain PFAS because

[1]Department of Civil and Environmental Engineering, Clarkson University, Potsdam, NY, USA. [2]Department of Chemical and Environmental Engineering, University of California, Riverside, Riverside, CA, USA. [3]Institute for a Sustainable Environment, Clarkson University, Potsdam, NY, USA. ✉e-mail: jinyongl@ucr.edu; yanyang@clarkson.edu

https://doi.org/10.1038/s44221-024-00232-7

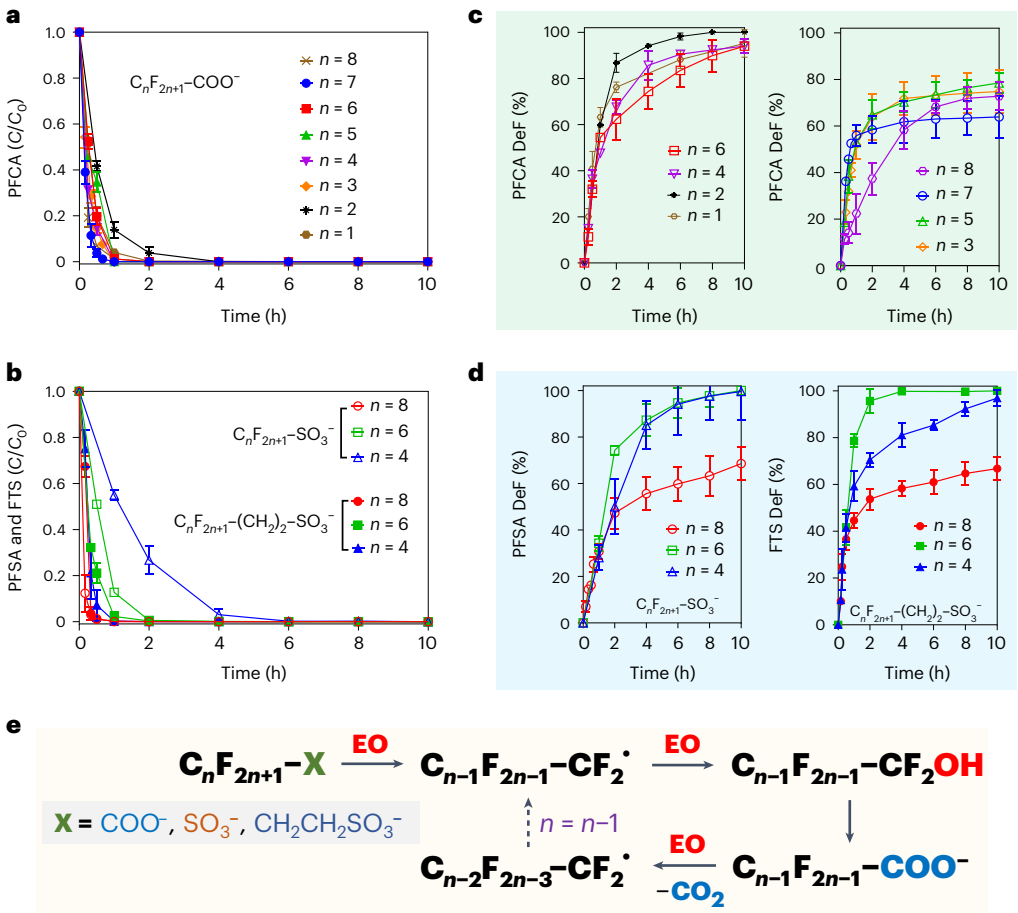

Fig. 1 | EO destruction and defluorination of individual PFAS. a–d, Parent compound degradation of $n = 1–8$ PFCA (**a**) and $n = 4$, 6 and 8 PFSA and FTS (**b**). Defluorination of $n = 1–8$ PFCA (**c**) and $n = 4$, 6 and 8 PFSA and FTS (**d**). Reaction conditions: individual PFAS (25 μM, except 1,000 μM for trifluoroacetate for ease of F^- measurement) spiked in 20 ml water with 100 mM Na_2SO_4 as electrolyte; current density of 15 mA cm^{-2} applied to a 16 cm^2 BDD anode. Data are presented as mean values of triplicates ± standard deviation. **e**, The previously known 'zipping-off' pathway.

they do not accumulate at the reactive gas–liquid interface[16,19,20]. Previously reported heterogeneous electrochemical oxidation (EO) treatment also exhibited various mass transfer and reactivity limitations in destroying individual PFAS structures[21–23]. The high amounts of organic solvents and hydrocarbon surfactants in AFFF further challenge the efficacy and efficiency of PFAS destruction systems[24].

Building on insights into both UV/S and EO technologies, we developed a UV/S–EO tandem process to maximize strength and overcome the limitations of each module. At ambient temperature and pressure, the UV/S–EO treatment achieved ~100% defluorination efficiency (DeF) for various individual PFAS chemicals and mixed PFAS in diluted AFFF (1:50–1:5,000, corresponding to 2–200 mg l^{-1} of total fluorine (TF)). In this paper, we present the process design rationale, demonstrate the system performance and elucidate reaction mechanisms. The findings provide a widely applicable solution for mineralizing mixed PFAS in various water treatment scenarios.

Process design rationales

Our previous studies have revealed that UV/S is highly effective in destroying long-chain PFCAs and PFSAs ($n > 4$ for the $C_nF_{2n+1}–$ moiety) but sluggish for short-chain PFSAs and FTs ($n \leq 4$)[17]. Moreover, UV/S treatment alone cannot achieve complete defluorination for most structures. One of the major pathways, reductive hydrodefluorination (that is, $C–F + 2e_{aq}^- + H^+ \rightarrow C–H + F^-$), can generate products with segregated fluorocarbon moieties (for example, $–CF_2–CH_2–X$). EO with boron-doped diamond (BDD) electrodes has shown effective destruction of a wide range of PFCAs, PFSAs and FTs, with robust performance in various water matrices and lower sensitivity to PFAS structures than UV/S[21,25,26]. However, EO alone cannot achieve complete defluorination of individual PFAS or diluted AFFF (see the following sections). It appears that UV/S and EO mechanistically complement each other towards complete defluorination.

To probe the suitability of integrating UV/S and EO, we conducted density functional theory-based calculations to compare the electrochemical oxidizability of perfluorooctanoic acid (PFOA) anion ($C_7F_{15}–COO^-$) and its representative hydrodefluorinated product after UV/S treatment, $C_7F_{14}H–COO^-$. The results indicate that $C_7F_{14}H–COO^-$ is more vulnerable to EO than PFOA, as the activation enthalpy profile moves towards lower anodic potentials (Supplementary Text 1 and Supplementary Fig. 1). By contrast, the $C_7F_{14}H–COO^-$ degradation under UV/S treatment was much slower than that of PFOA[17,18]. Therefore, the tandem UV/S–EO treatment train is mechanistically favourable.

Besides molecular-level insights, a series of process engineering considerations also consolidate the system design that places UV/S before EO. If EO is placed before UV/S, the direct treatment of perfluorinated structures can generate short-chain PFCAs and other unknown products that UV/S cannot 100% defluorinate. Furthermore, EO treatment of diluted AFFF generates high amounts of high-density foams that can incur various operational challenges (Supplementary Fig. 2). However, the UV/S–EO layout effectively addresses these foaming issues (highlighted in the following sections). Finally, Na_2SO_3 added in UV/S can be an electrolyte and a source of sulfate radicals in the downstream EO treatment (Supplementary Fig. 5), thus minimizing chemical consumption.

https://doi.org/10.1038/s44221-024-00232-7

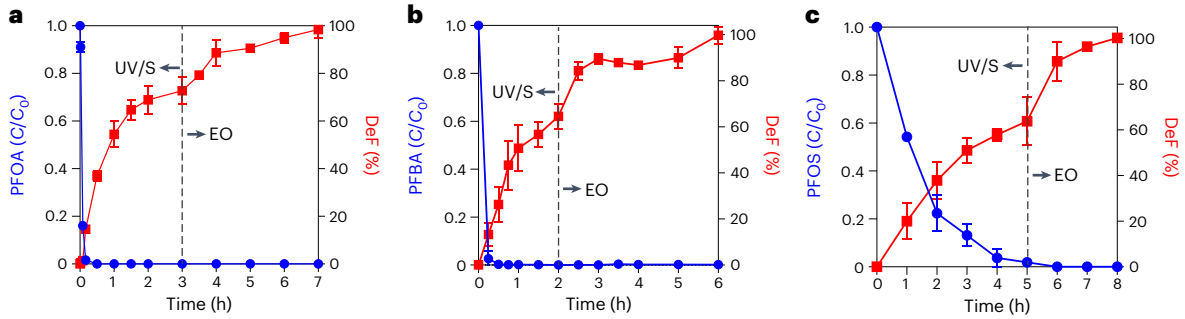

Fig. 2 | UV/S–EO treatment of selected PFAS. a–**c**, Degradation and defluorination of PFOA (**a**), PFBA (**b**) and PFOS (**c**). Reaction conditions for UV/S: individual PFAS (25 μM) spiked in 750 ml of water, 10 mM Na_2SO_3 and a 16 W low-pressure Hg lamp. The following EO treatment used the same conditions described in the caption of Fig. 1. Data are presented as mean values of triplicates ± standard deviation.

Structure–defluorination relationships in EO treatment

We used BDD, the gold standard in EO electrode materials, to treat the diverse PFAS and organic compounds in AFFF. This study used a plate-type microcrystalline BDD electrode (16 cm^2; Supplementary Fig. 3a) with dopant densities of 3×10^{20} boron atoms per cubic centimetre[27]. At a typical current density of 15 mA cm^{-2} used in this study, the anodic potential (corrected by uncompensated resistance) is ~3 V versus reversible hydrogen electrode (V_{RHE}) (Supplementary Fig. 4), surpassing the criteria for direct electron transfer oxidation of PFAS and the production of $HO^{\bullet}$ and $SO_4^{\bullet-}$ (refs. 28,29). Using perfluorooctane sulfonate (PFOS) destruction as the benchmark reaction, we confirmed that the EO system operated at the optimum electrode spacing, current density and (volume)/(electrode area) ratio (Supplementary Fig. 6). Applying these optimized conditions to treat other PFAS ensures an unbiased comparison of structure-dependent defluorination behaviours.

The first step was to systematically probe the structure–defluorination relationship for AFFF-relevant PFAS, including $n = 1$–8 C_nF_{2n+1}–COO^- (PFCA), $n = 4$, 6 and 8 C_nF_{2n+1}–SO_3^- (PFSA) and $n = 4$, 6 and 8 C_nF_{2n+1}–CH_2CH_2–SO_3^- (FTS). The BDD-based EO treatment showed excellent performance for all structures. Except for C_4F_9–SO_3^- (perfluorobutane sulfonate (PFBS)), most PFAS showed complete parent structure degradation within 2 h (Fig. 1a,b).

Electrolysis using BDD in sulfate-containing solutions can readily generate $HO^{\bullet}$ and $SO_4^{\bullet-}$ (refs. 30–33). However, these radicals hardly react with C_nF_{2n+1}–SO_3^- (refs. 34,35). Thus, the degradation must have been initiated by direct electron transfer from the PFSA molecule to the BDD electrode surface. The slower degradation of shorter PFSAs (Fig. 1b) can be attributed to their higher hydrophilicity in water. However, the same trend of mass transfer limitation was less prominent on short-chain $n = 1$–4 C_nF_{2n+1}–COO^- because, in addition to direct electron transfer oxidation, electrochemically generated $SO_4^{\bullet-}$ can initiate PFCA degradation by decarboxylation (Supplementary Fig. 7)[32,36].

For EO treatment of PFCAs, $n = 1$, 2, 4 and 6 allowed higher defluorination than $n = 3$, 5, 7 and 8 (Fig. 1c). For PFSAs and FTSs, $n = 4$ and 6 of both categories allowed near-complete defluorination, whereas the two $n = 8$ structures were defluorinated by 65% (Fig. 1d). These disparities suggest that the reaction mechanisms go beyond the previously known 'zipping-off' mechanism (Fig. 1e)[37,28]. The odd/even number of $-CF_2-$ in PFCAs appears to have crucial effects on the gap from 100% defluorination (<10% for $n = 2$, 4 and 6 versus >20% for $n = 3$, 5 and 7 C_nF_{2n+1}–COO^-). It is also intriguing to observe much lower defluorination for all three $n = 8$ structures than their $n = 2$ and 4 analogues. Elucidating the underlying mechanisms requires the identification of products that constitute the remaining organofluorine, which goes beyond the scope of this work. However, we present some preliminary results exclusively on PFOS to facilitate follow-up studies (Supplementary Figs. 8 and 9).

Despite pending questions about organofluorine products, EO has overwhelming advantages over UV/S for the degradation of individual PFAS structures. The strongly oxidative environment rapidly destroyed $n = 4$ FTS and achieved >95% defluorination. However, this compound is highly recalcitrant under UV/S[18,36]. Moreover, compared with UV/S, EO achieved much faster (10 h versus >24 h) and deeper (~100% versus 78%) defluorination of PFBS[18,36]. Hence, EO has higher reactivity towards short-chain PFAS than two other technologies—plasma and sonication—both encountered challenges with PFBS (C_4F_9–SO_3^-) and perfluorobutanoic acid (PFBA) (C_3F_7–COO^-)[38,39].

On the basis of the above-mentioned experimental findings, we hypothesized that EO should be placed after UV/S for two reasons. First, EO can achieve ~100% defluorination of $n \leq 4$ short-chain FTS and PFSAs, which are resistant to UV/S treatment. Second, UV/S can defluorinate $n = 3$, 5, 7 and 8 PFAS and produce H-rich polyfluorinated residues, which are ideal substrates for 100% defluorination by EO destruction.

UV/S–EO treatment of individual PFAS

To validate the hypotheses mentioned above, we developed a primitive UV/S–EO layout to treat PFOS, PFOA and PFBA, all of which are representative PFAS and could not be 100% defluorinated by EO alone (Fig. 1). In the UV/S treatment step, PFOA and PFBA were completely removed within 30 min (Fig. 2a,b). We arbitrarily stopped the UV/S treatment after 2–3 h when the increase in defluorination became sluggish. The following EO treatment increased defluorination to 100% for all three PFAS.

The UV/S treatment of $n = 7$ PFOA generated a series of shorter-chain $n = 1$–6 PFCAs (Fig. 3a). These PFCAs are attributed to well-known decarboxylation[17] and C–C bond cleavage mechanisms[40]. The UV/S treatment removed most of the PFCA transformation products within 3 h. Quadruple time-of-flight high-resolution mass spectrometry (Q-ToF-HRMS) detected a series of hydrodefluorination products (Fig. 3b) and the chain-shortened perfluoroheptanoic acid (PFHpA) ($C_7F_{13}O_2^-$). The MS peaks for $C_8HF_{14}O_2^-$ and PFHpA showed similar abundance (Fig. 3b), indicating that the two transformation pathways proceeded in parallel and were equally important (Fig. 3c). The H/F exchange may first occur on the alpha carbon due to the weakest C–F bond[17]. Regarding deep hydrodefluorination that left three C–F bonds uncleaved (for example, $C_8H_{12}F_3O_2^-$ and $C_7H_{10}F_3O_2^-$), the most probable transformation product structure may have a terminal CF_3^-, with all other carbons carrying C–H bonds. This is because terminal CF_3- has stronger C–F bonds (bond dissociation energy > 120 kcal mol^{-1}) than those in $-CF_2-$ (106–111 kcal mol^{-1}) and –CFH– (101–110 kcal mol^{-1})[36].

The UV/S degradation of hydrofluorinated transformation products, such as $C_8HF_{14}O_2^-$ and $C_8H_2F_{13}O_2^-$, was much slower than perfluorinated PFOA (Fig. 3b versus Fig. 2a). Switching to EO mode generated short-chain PFCAs from various hydrodefluorinated transformation

https://doi.org/10.1038/s44221-024-00232-7

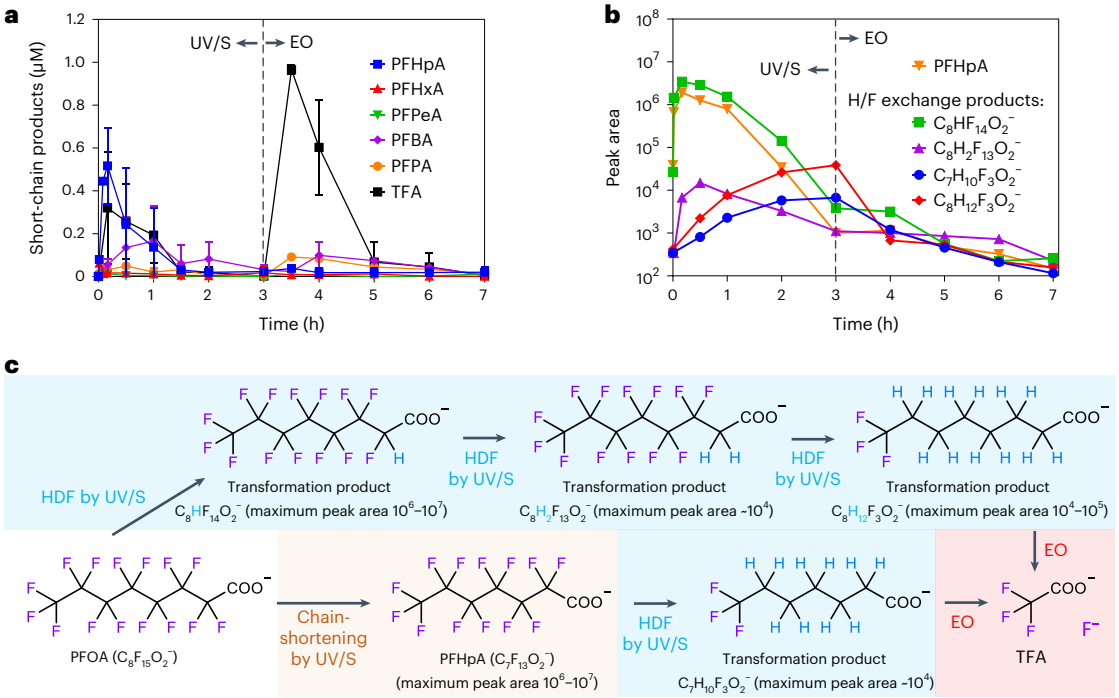

Fig. 3 | Evolution of detected transformation products during the UV/S–EO treatment of 25 μM PFOA. a,**b**, Targeted analysis of short-chain PFCA intermediates (**a**) and non-target analysis of hydrodefluorinated products (**b**). Data in **a** are presented as mean values of triplicates ± standard deviation. Data in **b** are mean values of duplicates. **c**, Formation pathways for representative products. HDF, hydrodefluorination.

products (Fig. 3a). A sharp increase in trifluoroacetate suggested that hydrodefluorination by UV/S occurred on carbon atoms near the terminal CF_3^-. With the extension of EO treatment, all PFCA transformation products (Fig. 3a) and hydrodefluorinated transformation products (Fig. 3b) were reduced to negligible concentrations, as evidenced by achieving ~100% defluorination (Fig. 2a).

UV/S–EO treatment of AFFF

The near-quantitative defluorination of individual PFAS structures motivated us to apply UV/S–EO for AFFF treatment at ambient conditions. This study focused on the treatment of fluorotelomerization-derived AFFF products ('Buckeye 3%' and 'Ansulite 6%', respectively, denoted as Buckeye and Ansulite below), which are still being used and causing downstream PFAS contamination[41]. For fire suppression, the AFFF product is typically diluted about 100-fold. It is further diluted after entering the water environment. Therefore, in this study, the AFFF products were diluted at various ratios with different water matrices. So far, only a few studies have reported treating diluted AFFF ([TF] = 0.16–27 mg l^{-1}) by individual EO, UV/S and plasma technologies[10,22,24,42]. None of the methods operated at ambient conditions realized ~100% defluorination (Supplementary Table 1).

The [TF] values in the original Buckeye AFFF and Ansulite AFFF were measured as 10.1 and 6.1 g l^{-1}, respectively, by combustion ion chromatography (Supplementary Table 2). Because no fluoride (F^-) was detected in these AFFF products, the [TF] represents the total organic fluorine concentration. Nineteen of the 30 targeted PFAS structures were detected in Buckeye AFFF (Supplementary Table 3). The three most abundant targeted PFAS were 6:2 FTS (139 mg l^{-1}), 8:2 FTS (7.85 mg l^{-1}) and PFOA (3.54 mg l^{-1}). In Ansulite, 6:2 FTS is the dominant PFAS as well. F elements from all targeted PFAS accounted for only 2% of the TF in Buckeye AFFF (0.4% for Ansulite). ^{19}F nuclear magnetic resonance (^{19}F NMR) analysis also found the dominant species in Buckeye AFFF as n = 6 FT surfactants (that is, C_6F_{13}–$(CH_2)_m$–R_O, Supplementary Fig. 10).

Under UV/S treatment of the 100-fold diluted Buckeye AFFF ([TF] at 100 mg l^{-1}), the concentration of 6:2 FTS increased in the first 8 h and then slowly decreased (Fig. 4a). PFSAs such as the n = 6 perfluorohexane sulfonate (PFHxS) showed a similar generation-degradation profile (Fig. 4b). The slow apparent degradation of these species can be attributed to (1) competing species in the organic matrix of diluted AFFF[24] and (2) the continuous generation of PFHxS from n = 6 sulfonamide surfactant precursors. This reasoning is further supported by the rather consistent concentration of PFOS, which has higher reactivity than PFHxS in previous UV/S studies[36]. The sustained PFOS throughout the 24 h is most probably attributed to the conversion of n = 8 sulfonamide precursors. PFCAs also showed generation-degradation patterns under UV/S treatment (Fig. 4c). Because the initial concentrations of all PFCAs were negligible, the generated PFCAs could be attributed to the conversion of fluorotelomeric and sulfonamide precursors[17]. A series of n = 4–7 surfactant molecules (detected by Q-ToF-HRMS following ref. 10) demonstrated high recalcitrance or even a net increase (Supplementary Fig. 11). The UV/S treatment resulted in 40% overall defluorination after 24 h (Fig. 4d). Extended reaction beyond 24 h did not further increase defluorination (Supplementary Fig. 12).

Note that we used a commercial UV reactor (750 ml) as the platform for the UV/S process. To demonstrate the scaled-up EO treatment, we used a commercial EO flow cell to receive all 750 ml UV/S-treated water. The flow cell was equipped with a BDD anode, similar to the BDD plate used in the degradation of individual PFAS (Figs. 1–3). Using PFOS destruction as the benchmark reaction, the flow cell operation was optimized to align the performance with the plate-type reactor (Supplementary Fig. 13).

After switching to EO mode, all surfactant molecules degraded to non-detectable levels after 40 h (that is, 16 h under EO, Supplementary Fig. 11). In comparison, most targeted PFAS structures showed concentration increases (Fig. 4a–c) and eventually became non-detectable after 44 h (that is, 20 h under EO). The early generation of n = 5 perfluorohexanoic acid (PFHxA), n = 4 perfluoropentanoic acid (PFPeA) and n = 3 PFBA in high concentrations suggests the oxidative conversion of the dominant n = 6 FT precursors, as revealed by ^{19}F NMR (Supplementary Fig. 10). The second wave of PFCA generation started

https://doi.org/10.1038/s44221-024-00232-7

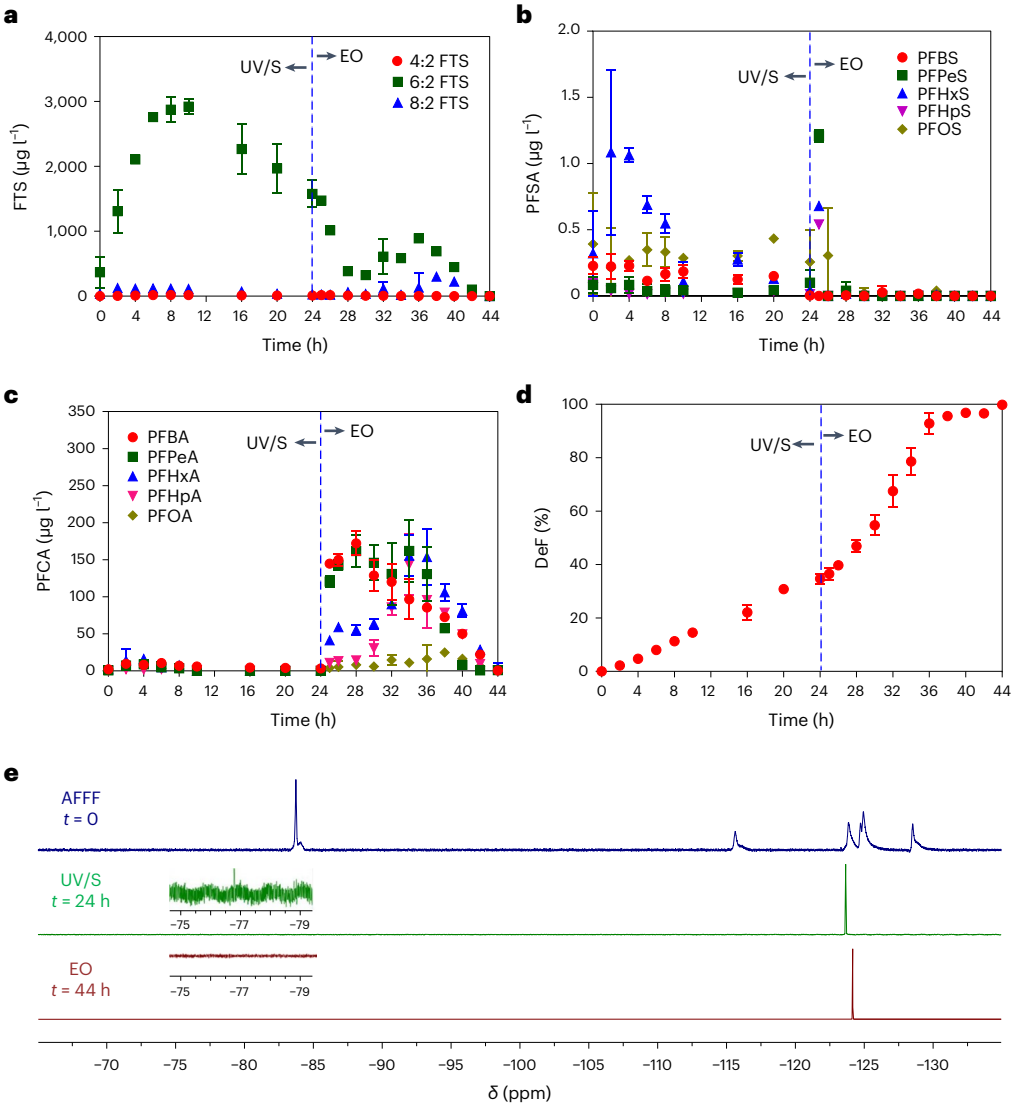

Fig. 4 | UV/S–EO treatment of AFFF. a–d, Time profiles of FTS (**a**), PFSA (**b**), PFCA (**c**) and defluorination (**d**) during UV/S–EO treatment of AFFF (Buckeye 3%; 1:100 diluted in DI water; [TF] = 102 mg l^{-1}). Reaction conditions for UV/S: 750 ml water, 100 mM Na_2SO_3, pH 12 by NaOH and a 16 W low-pressure Hg lamp. The EO treatment (no Na_2SO_4 added) was conducted in a BDD flow cell at a current of 5 A and an average cell voltage of 25 V. Data are presented as mean values of triplicates ± standard deviation. **e**, ^{19}F NMR analysis of AFFF samples derived from the treatment process.

after 32 h, with the notable increase for $n = 6$ PFHpA, followed by $n = 5$ PFHxA and 7 PFOA, suggesting a slower oxidative conversion of $n = 8$ FT precursors[34,36]. The very short time window for PFSAs (Fig. 4b) further confirmed that sulfonamide precursors were minor components in the studied AFFF, and all degraded within a few hours. After the EO treatment, all targeted PFAS were below the detection limits shown in Supplementary Table 3. The F^- ion release reached ~100% of overall defluorination (Fig. 4d). ^{19}F NMR analysis of the residual also found no other F resonance besides F^- (Fig. 4e), which is another evidence for near-quantitative defluorination. As a control test, we demonstrated that EO alone could not achieve 100% defluorination of diluted AFFF (for more discussion, see Supplementary Fig. 14).

Engineering considerations for AFFF treatment by UV/S–EO

TOC removal

Total organic carbon (TOC) analysis of the 100-fold diluted AFFF found 1,882 mg l^{-1} of organic carbon (Fig. 5a). However, after UV/S treatment, the measured TOC increased to 2,175 mg l^{-1}. Notably, the default combustion temperature (680 °C) of the TOC analyser cannot thoroughly oxidize all carbons, especially the fluorinated carbons, into CO_2. Hence, UV/S treatment converted the 'combustion-proof' mixed surfactants into more thermally oxidizable structures. After EO treatment, TOC was drastically reduced to only 13 mg l^{-1}. Assuming the value of 2,175 mg l^{-1} was similar to or still lower than the actual TOC of the 100-fold diluted AFFF, the TOC removal by EO was ≥99.4%. Because fluorinated carbon that accommodates 100 mg l^{-1} of organic F as $-CF_2-$ and CF_3- was only a small portion of TOC, we concluded that EO treatment allows deep mineralization of most hydrocarbon surfactants.

Foam suppression

To quantitatively describe foaming, we arbitrarily defined the 'foaming potential' as the ratio between the height of foam and the depth of liquid under air purging at 100 ml min^{-1}. Note that this is an ex situ characterization of samples before and after treatment. The raw 100-fold diluted AFFF had a foaming potential of 6 (Fig. 5b). After UV/S treatment, the value decreased to 1.4 (Fig. 5c). UV/S treatment can substantially alter the PFAS structures, such as H/F exchange, introducing additional carboxylate and sulfonate groups, and C–C bond cleavage to form shorter-chain transformation products[40].

https://doi.org/10.1038/s44221-024-00232-7

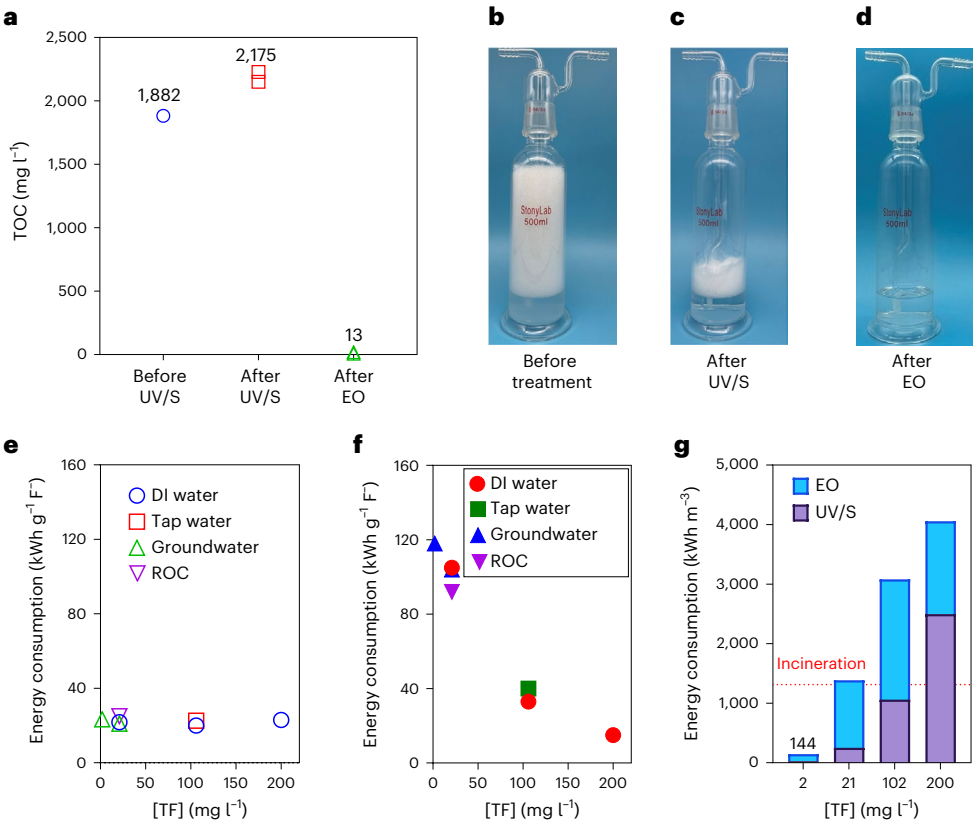

Fig. 5 | Advantages and engineering considerations of the UV/S–EO process. **a**, Measured TOC of the 100-fold diluted Buckeye AFFF by DI water before and after treatment. **b**–**d**, Foaming potentials of the 100-fold diluted Buckeye AFFF in DI water before treatment (**b**), after UV/S pretreatment (**c**) and after EO treatment (**d**). The 500 ml gas washing bottle was loaded with 70 ml of each water sample. Air was purged through the glass frit immersed in the aqueous phase (2.5 cm deep) until a stable foam layer was observed. The heights of the foam layer for the three samples were 15 cm (**b**), 3.6 cm (**c**) and 0 cm (**d**). **e**,**f**, Energy consumption for defluorination of UV/S (**e**) and the following EO at different [TF] (**f**). **g**, Overall energy consumption to achieve ~100% defluorination at different [TF].

Such transformations might lower the hydrophobicity and, thus, the foaming potential[43].

In the treatment operation, the UV/S process did not produce foam, as there was no gas evolution involved. The UV/S treatment to reduce foaming potential allows for easy operation of EO treatment. We observed only a thin foam layer with a height of less than 8% of the liquid in the first 4 h and no foaming after that. As expected from the ≥99.4% TOC removal, the foaming potential became 0 after the EO treatment (Fig. 5d). Therefore, the sequential UV/S–EO has a unique advantage in addressing the foaming issue from AFFF treatment.

Robustness in real-world scenarios

An imminent application scenario for UV/S–EO is the cleaning of hanger firefighting pipelines and fire trucks that have used PFAS-based AFFF in recent decades[7,8]. We used tap water for 100-fold dilution of Buckeye AFFF (Supplementary Table 2). The UV/S–EO treatment resulted in similar evolution/degradation kinetics for all individual PFAS and F^- release (Supplementary Fig. 15) compared with the deionized (DI) water-diluted AFFF (Fig. 4). We also observed similar reaction kinetics for all species at dilution factors of 50 (Supplementary Fig. 16) and 500 (Supplementary Fig. 17), except that more diluted (that is, less concentrated) AFFF needed less time to achieve 100% defluorination. For the UV/S module, energy consumption appeared proportional to the dilution factor. The treatment of 500-fold diluted AFFF needed 10 mM sulfite and 12 h to reach the maximum defluorination of 46% (Supplementary Fig. 17d). For the 50-fold diluted AFFF, 100 mM sulfite and 120 h were needed to reach the maximum defluorination of 48% (Supplementary Fig. 16d). In comparison, the EO module is less sensitive to the dilution factor. The time required to achieve 100% overall defluorination for 50- and 500-fold diluted AFFF was 24 and 12 h, respectively. It is important to highlight that the 50-fold diluted AFFF had a high TOC of 3,764 mg l^{-1} and TF of 200 mg l^{-1} compared with samples treated in previous studies (Supplementary Table 1). Hence, UV/S–EO has demonstrated great promise in destroying concentrated PFAS in wastewater, particularly addressing the major challenges in firefighting system cleaning.

To explore more application potentials, we deployed the UV/S–EO process in treating Buckeye AFFF diluted with groundwater and reverse osmosis concentrate (ROC; derived from groundwater remediation practice) at a 500-fold dilution. Despite differences in ionic composition and background organic content (Supplementary Table 2), ~100% defluorination was realized in both water matrices (Supplementary Figs. 18 and 19). Furthermore, UV/S–EO treatment of a different brand of AFFF, Ansulite, was conducted. The Ansulite AFFF was diluted 60-fold to yield a [TF] of 102 mg l^{-1}, close to that (103 mg l^{-1}) of 500-fold diluted Buckeye AFFF. Complete defluorination was also achieved (Supplementary Fig. 20). Finally, the UV/S–EO process was applied to treat 5,000-fold diluted Buckeye AFFF by groundwater ([TF] = 2 mg l^{-1}). In this scenario, the [FTS] values commensurate with reported AFFF-impacted groundwater[41,24]. Near-complete (~100%) defluorination was again achieved after 4 h of treatment (Supplementary Fig. 21).

The successful demonstration of ~100% defluorination of AFFF diluted in different water matrices within a wide [TF] window (2–200 mg l^{-1}) indicates that UV/S–EO is a universal and robust strategy applicable to various contamination scenarios. The UV/S–EO could be readily incorporated into a treatment train. It would be case-specific for practitioners to decide (based on PFAS concentration, sample volume and treatment duration) whether a separation/concentration process would be needed.

Energy consumptions

We calculated the energy efficiency of UV/S and EO modules based on the slopes of the quasi-linear segments of the defluorination profiles (Fig. 4d and Supplementary Figs. 15d, 16d, 17d, 18d, 19d, 20d and 21d) as the required energy input (kWh) to convert per gram of the organic fluorine to F^- (Fig. 5e,f). Light-adsorbing water matrices are usually expected to limit the efficacy of photochemical systems[44], but the UV/S system exhibited consistent energy efficiency for the 50-, 100-, 500- and 5,000-fold-diluted Buckeye AFFF. In particular, the UV/S treatment further reduced the absorbance at 254 nm in the 50-fold diluted AFFF from 1.36 to 0.36 (Supplementary Table 4). This 'self-sharpening' feature makes UV/S suitable for treating concentrated AFFF. The lowest dilution factor of 1:50 in this work is three orders of magnitude lower (that is, three orders of magnitude more concentrated) than the previous UV/S demonstration, which diluted AFFF 60,000-fold and operated at pH 9.5 (ref. 24). The limited dilution substantially reduced the water volume to be treated, thus saving substantial electrical energy for UV irradiation.

For EO treatment, energy consumption decreased with higher [TF]. This observation aligns with the principle of heterogeneous catalysis: higher bulk concentration creates a steeper concentration gradient at the water–electrode interface, thus enhancing the mass transfer of PFAS to the BDD surface and subsequent oxidation by direct electron transfer. Therefore, high [TF], though deemed challenging in many treatment processes, is highly beneficial for improving the electrical energy efficiency of the EO module.

Figure 5g shows the energy consumption in kWh m^{-3} to completely defluorinate AFFF by the UV/S–EO process. The data were acquired using UV/S to achieve a maximum defluorination of 40–50% and then complete the remaining defluorination by EO. The lowest energy consumption of 144 kWh m^{-3} was observed when treating diluted AFFF at [TF] of 2 mg l^{-1}. Energy consumption increases with the increase in [TF]. Meanwhile, the contribution of UV/S to energy consumption increases while that of EO decreases towards a higher [TF]. It is critical to highlight that this study realized 100% defluorination of diluted AFFF at ambient conditions. Thus, the energy consumption data set the groundwork for future process optimization.

Currently, AFFF disposal by incineration is facing many challenges. The US Department of Defense issued a temporary ban on incinerating PFAS-laden items, with particular emphasis on AFFF, starting on 26 April 2022. While the moratorium was lifted on 11 July 2023, there is still uncertainty about available qualified incineration facilities. Pilot-scale tests on AFFF incineration also indicate the formation of organofluorine incomplete combustion products, and ~100% defluorination was not reported[45]. The energy consumption of incineration was estimated at 1,312 kWh m^{-3} by calculating the energy demand to vaporize water to >1,100 °C (ref. 46). Seemingly, the energy consumption of UV/S–EO is higher than incineration when treating AFFF-impacted water at [TF] of 102 mg l^{-1} and above (Fig. 5g). However, the practice of AFFF incineration must address several challenges (waste transport to limited qualified facilities, high installation cost, stringent air emission control, public health concerns and so on) that could not be reflected in the primitive energy consumption comparison. Though a more comprehensive techno-economic analysis is warranted in future studies, we believe UV/S–EO is competitive in treating AFFF-impacted wastewater, given that on-site treatment using commercially viable modules is feasible, and complete defluorination can be achieved at ambient conditions.

Extended discussion towards practical applications

The UV/S–EO tandem process achieved the long-pursued goal of near-quantitative defluorination of PFAS as either individual chemicals or complex mixtures in AFFF matrices. All reactor components are commercially viable at full scale. Integration only requires conveying the treated effluents without retrofitting the reaction units. The substantial defluorination enables facile process control, as the plateau of fluoride evolution (that is, the turning point to switch UV/S to EO) can be monitored by F^--selective electrodes. We expect this treatment strategy to be also effective towards novel PFAS structures[40,47,48] in various practical scenarios under ambient conditions.

Finally, we emphasize that UV/S–EO was developed for the non-potable treatment of AFFF-laden water and wastewater. Therefore, concerns about disinfection by-products, which are only regulated in drinking water supplies, should not constrain the improvement and deployment of the process. Besides, technologies for removing halogenated by-products and oxyanions are emerging and can be adopted as post-treatment add-ons[29,49–51]. We are developing various engineering processes with pre- and post-treatment that can further expand the application scope of UV/S–EO in even more challenging water matrices.

Methods

Chemicals

Chemicals used as received include sodium sulfite (Sigma-Aldrich, ≥98%), sodium hydroxide (J.T.Baker, ≥99%), sodium sulfate (J.T.Baker, ≥98%), PFCAs (n = 1–8 $C_nF_{2n+1}COO^-$), PFSAs (n = 4, 6 and 8 $C_nF_{2n+1}SO_3^-$) and FTS (n = 4, 6 and 8 C_nF_{2n+1}–CH_2CH_2–SO_3^-). Information on CAS numbers, purities and vendors is presented in Supplementary Information (Supplementary Table 5). Two AFFF products, 'Buckeye 3%' and 'Ansulite 6%', were diluted using various water matrices (DI water, tap water, groundwater and ROC) to simulate different AFFF contamination scenarios. Tap water and groundwater were collected from Potsdam, New York. ROC of groundwater was collected from a PFAS-impacted site remediation project.

Analysis

Targeted analysis of PFAS was conducted using ultrahigh-performance liquid chromatography (Thermo Vanquish) coupled with triple quadrupole mass spectrometry (Thermo Altis). The analytical method includes 30 PFAS. Details of instrument set-up were described in our previous publication[52]. Non-targeted analysis of PFAS transformation products was performed using high-performance liquid chromatography-Q-ToF-MS (SCIEX). The instrument set-up is described in Supplementary Text 2. The search and match of unknown fluorocarbon structures followed the protocol developed previously[40].

The analysis of F^- was conducted on a Dionex Aquion ion chromatography system with an anion-exchange column (Thermo Fisher Scientific, RFIC IonPac AS18 column). The AS18 column was used with a KOH solution (23 mM) as the eluent at a flow rate of 1 ml min^{-1}, and a suppressor current of 57 mA was applied. The detection limit of F^- is 50 µg l^{-1}.

The TF of AFFF was analysed by combustion ion chromatography (Metrohm), with the principle of decomposing AFFF samples at 1,050 °C and using ion chromatography to measure the released F^-. Details were described previously[42,52].

The DeF for the treatment of a single PFAS target was calculated as follows:

$$\mathrm{DeF} = \frac{C_{F^-}}{C_0 \times N_{C-F}} \times 100\%$$

where C_{F^-} is the molar concentration of F^- ion released in solution, C_0 is the initial molar concentration of the parent PFAS and N_{C-F} is the number of C–F bonds in the parent PFAS molecule.

The DeF for the treatment of diluted AFFF was obtained via

$$\mathrm{DeF} = \frac{C_{F^-}}{C_{TF} - C_{F^-,0}} \times 100\%$$

where C_{TF} and $C_{F^-,0}$ are the concentrations of TF and F^- (if any) in the diluted AFFF, respectively.

UV/S treatment

A customized 750 ml stainless-steel photoreactor with a quartz UV-lamp sheath and a 16 W low-pressure Hg lamp (254 nm narrowband irradiation) was used for UV/S treatment. The photon flux ($1.3 \pm 0.2 \times 10^{-6}$ E s^{-1}), effective path length (27 cm) and average intensity (5.4×10^{-8} E s^{-1} cm^{-2}) were determined using established methods (Supplementary Text 3)[53]. For the UV/S treatment of a single PFAS, DI water was spiked with 25 μM target PFAS and 10 mM Na_2SO_3. The pH was adjusted to 12 by 1 M NaOH to achieve the highest photo-reductive treatment efficiency[54]. As for the UV/S treatment of AFFF, AFFF samples diluted by DI water or tap water at ratios of 1 to 50, 1 to 100 and 1 to 500 were amended with Na_2SO_3 at 100, 100 and 10 mM, respectively. The reactor was sealed from air exposure without inert gas protection in all tests.

EO treatment

EO treatment based on plate-type BDD (Element Six; Supplementary Fig. 3a) aimed to evaluate the treatability of target PFAS with or without UV/S pretreatment. In these tests, 20 ml PFAS-containing electrolytes with or without UV/S pretreatment were electrolysed in batch mode by a 16 cm^2 BDD anode coupled with a stainless-steel cathode at 15 mA cm^{-2}, corresponding to a total current of 0.24 A.

To establish the proof-of-concept UV/S–EO tandem treatment train, we adopted a BDD flow cell for larger treatment capability. The BDD flow cell reactor, provided by Element Six, contains two BDD disks (4.4 cm diameter each with an interspace of 0.8 cm) that serve as anode and cathode (Supplementary Fig. 3b). The flow cell has a chamber volume of 95 ml. In the tandem treatment process, 750 ml of diluted AFFF is first subjected to UV/S reductive treatment; the 750 ml treated water is then circulated through the flow cell at a flow rate of 100 ml min^{-1}. It is important to note that the batch EO tests using plate-type BDD have a current-to-volume ratio of 12 A l^{-1}. If the same ratio is replicated in the flow cell set-up, the required total current would be 9 A to treat 750 ml. However, limited by the capacity of the bench-scale power supply, the flow cell was operated at 5 A, corresponding to a current density of 329 mA cm^{-2}. The near-complete defluorination of AFFF was achieved in the compromised condition, nonetheless. When taking samples, the power was turned off, and water continued to be recirculated until foam (if any) dissipated.

Data availability

The data that support the findings of this study are available within the paper and its Supplementary Information. Source data for all graphs are provided in this paper.

References

1. Evich, M. G. et al. Per- and polyfluoroalkyl substances in the environment. *Science* **375**, eabg9065 (2022).
2. Moody, C. A. & Field, J. A. Perfluorinated surfactants and the environmental implications of their use in fire-fighting foams. *Environ. Sci. Technol.* **34**, 3864–3870 (2000).
3. Awad, E. et al. Long-term environmental fate of perfluorinated compounds after accidental release at Toronto airport. *Environ. Sci. Technol.* **45**, 8081–8089 (2011).
4. Hu, X. C. et al. Detection of poly- and perfluoroalkyl substances (PFASs) in US drinking water linked to industrial sites, military fire training areas, and wastewater treatment plants. *Environ. Sci. Technol. Lett.* **3**, 344–350 (2016).
5. Mejia-Avendaño, S. et al. Novel fluoroalkylated surfactants in soils following firefighting foam deployment during the Lac-Megantic railway accident. *Environ. Sci. Technol.* **51**, 8313–8323 (2017).
6. Liu, M., Munoz, G., Vo Duy, S., Sauvé, S. & Liu, J. Per- and polyfluoroalkyl substances in contaminated soil and groundwater at airports: a Canadian case study. *Environ. Sci. Technol.* **56**, 885–895 (2021).
7. Cornelsen, M., Weber, R. & Panglisch, S. Minimizing the environmental impact of PFAS by using specialized coagulants for the treatment of PFAS polluted waters and for the decontamination of firefighting equipment. *Emerg. Contam.* **7**, 63–76 (2021).
8. Lang, J. R. et al. Characterization of per- and polyfluoroalkyl substances on fire suppression system piping and optimization of removal methods. *Chemosphere* **308**, 136254 (2022).
9. Krause, M. J. et al. Supercritical water oxidation as an innovative technology for PFAS destruction. *J. Environ. Eng.* **148**, 05021006 (2022).
10. Hao, S. et al. Hydrothermal alkaline treatment for destruction of per- and polyfluoroalkyl substances in aqueous film-forming foam. *Environ. Sci. Technol.* **55**, 3283–3295 (2021).
11. Pinkard, B. R. Aqueous film-forming foam treatment under alkaline hydrothermal conditions. *J. Environ. Eng.* **148**, 05021007 (2022).
12. Place, B. J. & Field, J. A. Identification of novel fluorochemicals in aqueous film-forming foams used by the US military. *Environ. Sci. Technol.* **46**, 7120–7127 (2012).
13. D'Agostino, L. A. & Mabury, S. A. Identification of novel fluorinated surfactants in aqueous film forming foams and commercial surfactant concentrates. *Environ. Sci. Technol.* **48**, 121–129 (2014).
14. Barzen-Hanson, K. A. et al. Discovery of 40 classes of per- and polyfluoroalkyl substances in historical aqueous film-forming foams (AFFFs) and AFFF-impacted groundwater. *Environ. Sci. Technol.* **51**, 2047–2057 (2017).
15. Park, H. et al. Reductive defluorination of aqueous perfluorinated alkyl surfactants: effects of ionic headgroup and chain length. *J. Phys. Chem. A* **113**, 690–696 (2009).
16. Campbell, T. Y., Vecitis, C. D., Mader, B. T. & Hoffmann, M. R. Perfluorinated surfactant chain-length effects on sonochemical kinetics. *J. Phys. Chem. A* **113**, 9834–9842 (2009).
17. Bentel, M. J. et al. Defluorination of per- and polyfluoroalkyl substances (PFASs) with hydrated electrons: structural dependence and implications to PFAS remediation and management. *Environ. Sci. Technol.* **53**, 3718–3728 (2019).
18. Liu, Z. et al. Accelerated degradation of perfluorosulfonates and perfluorocarboxylates by UV/sulfite+iodide: reaction mechanisms and system efficiencies. *Environ. Sci. Technol.* **56**, 3699–3709 (2022).
19. Singh, R. K. et al. Removal of poly- and per-fluorinated compounds from ion exchange regenerant still bottom samples in a plasma reactor. *Environ. Sci. Technol.* **54**, 13973–13980 (2020).
20. Li, R., Isowamwen, O. F., Ross, K. C., Holsen, T. M. & Thagard, S. M. PFAS–CTAB complexation and its role on the removal of PFAS from a lab-prepared water and a reverse osmosis reject water using a plasma reactor. *Environ. Sci. Technol.* **57**, 12901–12910 (2023).
21. Zhuo, Q. et al. Degradation of perfluorinated compounds on a boron-doped diamond electrode. *Electrochim. Acta* **77**, 17–22 (2012).
22. Schaefer, C. E. et al. Electrochemical transformations of perfluoroalkyl acid (PFAA) precursors and PFAAs in groundwater impacted with aqueous film forming foams. *Environ. Sci. Technol.* **52**, 10689–10697 (2018).
23. Liang, S. et al. Field demonstration of coupling ion-exchange resin with electrochemical oxidation for enhanced treatment of per- and polyfluoroalkyl substances (PFAS) in groundwater. *Chem. Eng. J. Adv.* **9**, 100216 (2022).
24. Tenorio, R. et al. Destruction of per- and polyfluoroalkyl substances (PFASs) in aqueous film-forming foam (AFFF) with UV–sulfite photoreductive treatment. *Environ. Sci. Technol.* **54**, 6957–6967 (2020).

25. Gomez-Ruiz, B. et al. Efficient electrochemical degradation of poly- and perfluoroalkyl substances (PFASs) from the effluents of an industrial wastewater treatment plant. *Chem. Eng. J.* **322**, 196–204 (2017).
26. Schaefer, C. E. et al. Electrochemical treatment of perfluorooctanoic acid and perfluorooctane sulfonate: insights into mechanisms and application to groundwater treatment. *Chem. Eng. J.* **317**, 424–432 (2017).
27. Macpherson, J. V. A practical guide to using boron doped diamond in electrochemical research. *Phys. Chem. Chem. Phys.* **17**, 2935–2949 (2015).
28. Radjenovic, J., Duinslaeger, N., Avval, S. S. & Chaplin, B. P. Facing the challenge of poly- and perfluoroalkyl substances in water: is electrochemical oxidation the answer? *Environ. Sci. Technol.* **54**, 14815–14829 (2020).
29. Yang, Y. Recent advances in the electrochemical oxidation water treatment: spotlight on byproduct control. *Front. Environ. Sci. Eng.* **14**, 85 (2020).
30. Shin, Y.-U. et al. Electrochemical oxidation of organics in sulfate solutions on boron-doped diamond electrode: multiple pathways for sulfate radical generation. *Appl. Catal. B* **254**, 156–165 (2019).
31. Yang, S., Fernando, S., Holsen, T. M. & Yang, Y. Inhibition of perchlorate formation during the electrochemical oxidation of perfluoroalkyl acid in groundwater. *Environ. Sci. Technol. Lett.* **6**, 775–780 (2019).
32. Liu, Y. et al. Enhanced perfluorooctanoic acid degradation by electrochemical activation of sulfate solution on B/N codoped diamond. *Environ. Sci. Technol.* **53**, 5195–5201 (2019).
33. Farhat, A., Keller, J., Tait, S. & Radjenovic, J. Removal of persistent organic contaminants by electrochemically activated sulfate. *Environ. Sci. Technol.* **49**, 14326–14333 (2015).
34. Houtz, E. F. & Sedlak, D. L. Oxidative conversion as a means of detecting precursors to perfluoroalkyl acids in urban runoff. *Environ. Sci. Technol.* **46**, 9342–9349 (2012).
35. Lutze, H. V., Brekenfeld, J., Naumov, S., von Sonntag, C. & Schmidt, T. C. Degradation of perfluorinated compounds by sulfate radicals—new mechanistic aspects and economical considerations. *Water Res.* **129**, 509–519 (2018).
36. Liu, Z. et al. Near-quantitative defluorination of perfluorinated and fluorotelomer carboxylates and sulfonates with integrated oxidation and reduction. *Environ. Sci. Technol.* **55**, 7052–7062 (2021).
37. Niu, J., Li, Y., Shang, E., Xu, Z. & Liu, J. Electrochemical oxidation of perfluorinated compounds in water. *Chemosphere* **146**, 526–538 (2016).
38. Shende, T., Andaluri, G. & Suri, R. Chain-length dependent ultrasonic degradation of perfluoroalkyl substances. *Chem. Eng. J. Adv.* **15**, 100509 (2023).
39. Isowamwen, O., Li, R., Holsen, T. & Thagard, S. M. Plasma-assisted degradation of a short-chain perfluoroalkyl substance (PFAS): perfluorobutane sulfonate (PFBS). *J. Hazard. Mater.* **456**, 131691 (2023).
40. Gao, J. et al. Photochemical degradation pathways and near-complete defluorination of chlorinated polyfluoroalkyl substances. *Nat. Water* **1**, 381–390 (2023).
41. Houtz, E. F., Higgins, C. P., Field, J. A. & Sedlak, D. L. Persistence of perfluoroalkyl acid precursors in AFFF-impacted groundwater and soil. *Environ. Sci. Technol.* **47**, 8187–8195 (2013).
42. Singh, R. K. et al. Rapid removal of poly- and perfluorinated compounds from investigation-derived waste (IDW) in a pilot-scale plasma reactor. *Environ. Sci. Technol.* **53**, 11375–11382 (2019).
43. Dalvi, V. H. & Rossky, P. J. Molecular origins of fluorocarbon hydrophobicity. *Proc. Natl Acad. Sci. USA* **107**, 13603–13607 (2010).
44. Crittenden, J. C., Trussell R. R., Hand, D. W., Howe, K. J. & Tchobanoglous, G. *MWH's Water Treatment: Principles and Design* (John Wiley & Sons, 2012).
45. Shields, E. P. et al. Pilot-scale thermal destruction of per- and polyfluoroalkyl substances in a legacy aqueous film forming foam. *ACS ES&T Eng.* **3**, 1308–1317 (2023).
46. Maga, D., Aryan, V. & Bruzzano, S. Environmental assessment of various end-of-life pathways for treating per- and polyfluoroalkyl substances in spent fire-extinguishing waters. *Environ. Toxicol. Chem.* **40**, 947–957 (2021).
47. Gao, J. et al. Defluorination of omega-hydroperfluorocarboxylates (ω-HPFCAs): distinct reactivities from perfluoro and fluorotelomeric carboxylates. *Environ. Sci. Technol.* **55**, 14146–14155 (2021).
48. Bentel, M. J. et al. Degradation of perfluoroalkyl ether carboxylic acids with hydrated electrons: structure–reactivity relationships and environmental implications. *Environ. Sci. Technol.* **54**, 2489–2499 (2020).
49. Gao, J., Xie, S., Liu, F. & Liu, J. Preparation and synergy of supported Ru_0 and Pd_0 for rapid chlorate reduction at pH 7. *Environ. Sci. Technol.* **57**, 3962–3970 (2023).
50. Ren, C., Bi, E. Y., Gao, J. & Liu, J. Molybdenum-catalyzed perchlorate reduction: robustness, challenges, and solutions. *ACS ES&T Eng.* **2**, 181–188 (2022).
51. Liu, J. & Gao, J. Catalytic reduction of water pollutants: knowledge gaps, lessons learned, and new opportunities. *Front. Environ. Sci. Eng.* **17**, 26 (2022).
52. Yang, N. et al. Solvent-free nonthermal destruction of PFAS chemicals and PFAS in sediment by piezoelectric ball milling. *Environ. Sci. Technol. Lett.* **10**, 198–203 (2023).
53. Li, X. et al. Efficient reductive dechlorination of monochloroacetic acid by sulfite/UV process. *Environ. Sci. Technol.* **46**, 7342–7349 (2012).
54. Bentel, M. J. et al. Enhanced degradation of perfluorocarboxylic acids (PFCAs) by UV/sulfite treatment: reaction mechanisms and system efficiencies at pH 12. *Environ. Sci. Technol. Lett.* **7**, 351–357 (2020).

Acknowledgements

Financial support was provided by the Strategic Environmental Research and Development Program (ER22-3184 for Y.G., Z.L., N.Y., J.L. and Y.Y.) and the National Science Foundation (CBET-2120452 for S.Y., L.E.Q.-C. and Y.Y.). We thank S. Fernando and T. Holsen at Clarkson University for providing the Ansulite AFFF sample and the assistance in non-targeted PFAS analyses.

Author contributions

Y.G. conducted PFAS degradation experiments, analysed the data and drafted the paper. Z.L. conducted PFAS degradation and NMR analysis. N.Y., S.Y. and L.E.Q.-C. assisted in the liquid chromatography high-resolution tandem mass spectrometry analysis. J.L. and Y.Y. designed and supervised the research and revised the paper.

Competing interests

The authors declare no competing interests.

Additional information

Supplementary information The online version contains supplementary material available at https://doi.org/10.1038/s44221-024-00232-7.

Correspondence and requests for materials should be addressed to Jinyong Liu or Yang Yang.

Peer review information *Nature Water* thanks Shilai Hao and the other, anonymous, reviewer(s) for their contribution to the peer review of this work.